JACS
JOURNAL OF THE AMERICAN CHEMICAL SOCIETY

ARTICLE

pubs.acs.org/JACS

Surface-Functionalization-Dependent Optical Properties of II−VI Semiconductor Nanocrystals

Ou Chen, Yongan Yang, Tie Wang, Huimeng Wu, Chenggang Niu, Jianhui Yang, and Y. Charles Cao*

Department of Chemistry, University of Florida, Gainesville, Florida 32611, United States

Supporting Information

ABSTRACT: We report a study of the surface-functionalization-dependent optical properties of II−VI zinc-blende semiconductor nanocrystals on the basis of ligand-exchange chemistry, isomaterial core/shell growth, optical spectroscopy, transmission electron microscopy, and X-ray powder diffraction. Our results show that the transition energy and extinction coefficient of the $2S_{h3/2}1S_e$ excitonic band of these nanocrystals can be strongly modified by their surface ligands as well as ligand associated surface atomic arrangement. The oleylamine exchange of oleate-capped zinc-blende II−VI nanocrystals narrows the energy gap between their first and second excitonic absorption bands, and this narrowing effect is size-dependent. The oleylamine exchange results in the quenching, subsequent recovery, and even enhancing of the photoluminescence emission of these II−VI semiconductor nanocrystals. In addition, the results from our X-ray powder diffraction measurements and simulations completely rule out the possibility that oleate-capped zinc-blende CdSe nanocrystals can undergo zinc-blende-to-wurtzite crystal transformation upon ligand exchange with oleylamine. Moreover, our theoretical modeling results suggest that the surface-functionalization-dependent optical properties of these semiconductor nanocrystals can be caused by a thin type II isomaterial shell that is created by the negatively charged ligands (e.g., oleate and octadecyl phosphonate). Taking all these results together, we provide the unambiguous identification that II−VI semiconductor nanocrystals exhibit surface-functionalization-dependent excitonic absorption features.

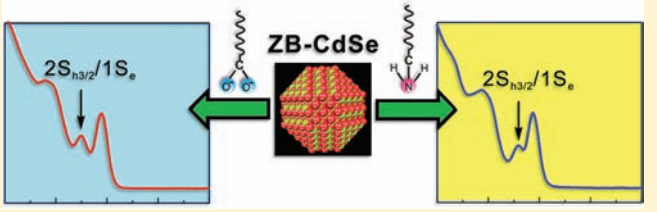

INTRODUCTION

The surface-dependent optical properties of colloidal semiconductor nanocrystals have been extensively studied in the past 2 decades.[1−10] It has been well-documented that the nature of nanocrystal surfaces can significantly modify photoluminescence (PL) properties of nanocrystals.[3,4,6−15] Defects on nanocrystal surface such as dangling bonds, adatoms, kinks, and vacancies often form shallow or deep trap states of electrons or holes, which can deactivate quantum-confined excitons via nonradiative or radiative pathways.[1−3,16] To date, a number of methods have been developed to passivate and control the surface of colloidal nanocrystals.[4−13] This advance has led to the preparation of a variety of high-quality colloidal nanocrystals with composition of II−VI, III−VI, and IV−VI semiconductors.[17−30] These colloidal nanocrystals exhibit narrow emission bands, high PL quantum yields, and high stability against oxidation and photo-oxidations. Some of these high-quality nanocrystals have been commercially available for practical applications, such as biological labels and LEDs.[31−37] In addition, nonblinking colloidal nanocrystals have been synthesized via surface passivation using thick and gradient shells.[6,7,38] With well-designed surface passivation, Guyot-Sionnest and co-workers have successfully synthesized core/shell semiconductor nanocrystals with a slow electron cooling rate, which are important to applications such as high-yield photovoltaics and IR sensors.[39] In this paper, we report that quantum-confined II−VI semiconductor nanocrystals exhibit surface-functionalization-dependent excitonic absorption features.

Size-dependent optical spectra of wurtzite (W) CdSe nanocrystals were identified by Norris et al. through a combination of experimental and theoretical analysis.[40] The major absorption features were assigned to the $1S_{h3/2}1S_e$ (E_1), $2S_{h3/2}1S_e$ (E_2), and $1P_{h3/2}1P_e$ (E_3) excitonic transitions. With the development of zinc-blende (ZB) CdSe nanocrystal synthesis, we and others found that the gap between the first (E_1, $1S_{h3/2}1S_e$) and second (E_2, $2S_{h3/2}1S_e$) exciton transition bands of ZB nanocrystals is larger than that of W ones, and the peak positions of the exciton transition bands with higher energies (e.g., E_3 and E_4) are also different between these two types of CdSe nanocrystals.[41−44] Although these two types of CdSe nanocrystals have different capping ligands (oleate for the ZB-CdSe particles and fatty amine for the W ones), this ligand difference was unfortunately ignored in previous studies of the optical properties of these nanocrystals.[41−44] We proposed that the differences between the absorption spectra of the ZB- and W-CdSe nanocrystals were due to their crystal structures because the corresponding bulk CdSe semiconductors have different electronic band structures at the center of the Brillouin zone.[41] Under this proposal, Mahler et al. have recently suggested that ZB-CdSe nanocrystals may undergo a surface-driven crystalline transition into W nanocrystals in a fatty-amine solution.[45] To further verify crystal-structure-dependent optical properties of CdSe nanocrystals, we studied the ligand exchange of ZB-

Received: September 3, 2011
Published: September 28, 2011

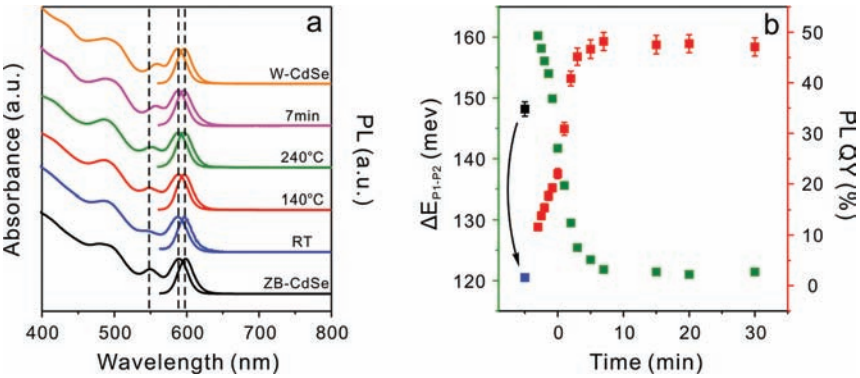

Figure 1. (a) Temporal evolution of the absorption and PL of the ZB-CdSe nanocrystals during the ligand exchange (from oleate to OAm) process. When the temperature or ligand exchange solution reached 240 °C, the time was counted as zero. (b) ΔE_{12} (green squares) and corresponding PL quantum yield (QY) (red squares) of the ZB-CdSe nanocrystals in the same reaction as in part a. The black square is the original PL QY of oleate-capped ZB-CdSe; the blue square is the PL QY of the oleate-capped ZB-CdSe mixed with OAm under ambient conditions.

CdSe nanocrystals using optical spectroscopy, transmission electron microscopy (TEM), and X-ray diffraction (XRD); we then carried out isomaterial core/shell growth of CdSe nanocrystals (e.g., to grow CdSe "shells" on the CdSe "core" nanocrystals) to probe the surface crystal structure of the ZB-CdSe nanocrystals after ligand exchange with oleylamine.

However, our results demonstrate that the absorption feature differences between the ZB-and W-CdSe nanocrystals are not due to their crystal structure, but instead depend on the surface functionalization related to their ligands (oleate vs oleylamine). These results clearly show that both the energy and absorption coefficient of the E_2 excitonic band (i.e., $2S_{h3/2}1S_e$) are dependent upon CdSe nanocrystal surface functionality. In addition, the ZB-CdS and ZB-CdTe nanocrystals exhibit similar surface-functionalization-dependent optical properties. Our theoretical analysis suggests that the surface-dependent absorption properties of II−VI semiconductor nanocrystals may originate from a thin type-II isomaterial shell associated with their ligand functionality. These results provide new insights into the optical properties of semiconductor nanocrystals, and the findings herein would be useful in the rational synthetic design of colloidal semiconductor nanocrystals with desired optical properties through surface functionalization.

RESULTS AND DISCUSSIONS

Ligand exchange of ZB-CdSe Nanocrystals with Oleylamine (OAm). We used 4.0-nm oleate-capped ZB-CdSe nanocrystals as a model system to study the evolution of the optical properties of CdSe nanocrystals during ligand exchange with OAm; 4.0-nm OAm-capped W-CdSe nanocrystals were used as the reference in our optical spectroscopic study. The ZB-CdSe nanocrystals (4.0 ± 0.2 nm in diameter) were synthesized using our previous method.[44] The W-CdSe nanocrystals (4.0 ± 0.2 nm in diameter) were prepared according to the method developed by Peng et al,[46] and a further ligand exchange was performed to maximize the OAm coverage on the W-CdSe nanocrystals (see Supporting Information). OAm exchange reactions of the oleate-capped ZB-CdSe nanocrystals were carried out in a 1:4 mixture of OAm and 1-octadecene (ODE) at 240 °C. This elevated temperature was used to promote the OAm exchange reactions.

To clearly assess OAm-induced surface effects on the optical properties of CdSe nanocrystals, one needs to minimize the oxidation, dissolution, and Ostwald ripening of these nanocrystals during this high-temperature ligand exchange, because these processes can lead to a significant blue- or red-shift of the excitonic bands of CdSe nanocrystals. In this study, we performed a thorough degassing treatment to maximize the oxygen removal from OAm exchange solutions via multiple freeze−pump−thaw operations. In addition, we introduced a large amount of ODE into the ligand exchange reaction to minimize amine-induced dissolution and/or Ostwald ripening of CdSe nanocrystals. It is known that amines lead to faceted etching and Ostwald ripening of CdSe nanocrystals at elevated temperatures through their complexation with the cadmium and/or selenium ions on the surface of CdSe nanocrystals.[47] The presence of ODE (a nonpolar solvent) in OAm-exchange solutions can decrease the solubility of the Cd/Se-OAm complexes through solvophobic interactions and thus reduce the dissolution and/or Ostwald ripening of CdSe nanocrystals. Indeed, our results show that OAm-exchange reactions in a mixture of OAm/ODE (4:1) resulted in a typical blue-shift of 9 nm in the E_1 excitonic band of 4.0-nm CdSe nanocrystals, whereas less than a 2 nm blue-shift of the E_1 band was observed in a typical exchange reaction in a mixture of OAm/ODE (1:4).

In a typical OAm-exchange reaction, a hexane solution containing 4.0-nm ZB-CdSe nanocrystals (25 nmol) was added into a thoroughly degassed mixture of OAm/ODE (1:4, 5 mL) at room temperature with stirring. After hexane was removed under vacuum, the resulting nanocrystal solution was heated under Ar to 240 °C, and then the solution was further annealed at this temperature for 30 min. Quantitative aliquots were periodically taken to study the optical property evolution of the ZB-CdSe nanocrystals during this OAm-exchange reaction.

After the ZB-CdSe nanocrystals were mixed with the OAm/ODE solution at room temperature, the peak position of their photoluminescence (PL) remained unchanged, but its intensity was significantly quenched; the PL quantum yield (QY) decreased from 35% to ~1.6% (Figure 1). These nanocrystals showed no measurable change in their E_1 absorption band but a substantial decrease (~25%) in the extinction coefficient (or oscillation strength) of their E_2 ($2S_{h3/2}1S_e$) band; this band appeared as a shoulder connected to their high-energy absorption bands (Figure 1). Without thermal treatment, no further change was observed in the optical properties of these CdSe nanocrystals for several months at room temperature.

With heating to 240 °C, however, these CdSe nanocrystals showed significant changes in their absorption and PL spectra. When the solution temperature reached 140 °C, the extinction

coefficient of their E_2 absorption band increased by ~12%, and the band reemerged as a peak located at the same wavelength (547 nm) as that of the ZB-CdSe nanocrystals before ligand exchange; their PL QY also increased to ~11% (Figure 1). With further increase of reaction temperature, the PL QY of these nanocrystals continuously increased; the E_2 absorption band of these particles gradually red-shifted, while their E_1 absorption band remained nearly unchanged, and thus the gap (i.e., ΔE_{12}) between these two bands narrowed continuously (Figure 1). The ΔE_{12} of ZB-CdSe nanocrystals was 161 meV before the OAm exchange reaction. When the solution temperature reached 240 °C, the ΔE_{12} of the nanocrystals decreased to 142 meV, and their PL QY increased to 22%. After annealing at 240 °C for 7 min, the resultant CdSe nanocrystals exhibited a PL QY of 48%, and their ΔE_{12} gap decreased to 121 meV, which is nearly identical to that of the 4.0-nm OAm-capped W-CdSe nanocrystals (Figure 1). At this stage, all absorption features of the CdSe nanocrystals almost perfectly resembled those of the W-CdSe nanocrystals (Figure 1). Further annealing did not lead to any measurable change in their optical bands or PL QY. Interestingly, the trend of increasing PL QY perfectly correlates with the trend of decreasing of the ΔE_{12} of the CdSe nanocrystals: the higher the PL QY of the CdSe nanocrystals, the narrower their ΔE_{12} gap. When their PL QY reached its maximum, the ΔE_{12} reached its minimum (Figure 1b). Moreover, the peak positions of their E_1 absorption band and PL emission were nearly unchanged during the ligand exchange.

These results clearly demonstrate that the OAm exchange of oleate-capped ZB-CdSe nanocrystals can result in nanocrystals with optical features nearly identical to those of OAm-capped W-CdSe nanocrystals. Although Mahler et al. have showed that OAm exchange can cause the ΔE_{12} gap narrowing, their results cannot make unambiguous identification of the fate of the E_2 excitonic peak of their nanocrystals because of the significant blue or red-shift in the E_1 peak of these nanocrystals.[45] In contrast, our data allow further identifying that the OAm exchange caused a red-shift of the E_2 absorption band of CdSe nanocrystals and induced the variations in the extinction coefficient of their E_2 band (Figure 1). In addition, our results show that, unlike W-CdSe nanocrystals, amine exchange of oleate-capped ZB-CdSe nanocrystals leads to a dramatic decrease in their PL QY at room temperature, which presents another interesting surface-dependent PL property of these nanocrystals (Figure 1).

FT-IR Spectroscopy. To further explore the origin of the unique features of the ZB-CdSe nanocrystals, we used FT-IR spectroscopy to study the bonding nature between ligands with the surface of the CdSe nanocrystals. Nanocrystal samples for IR measurements were taken at different stages in the typical OAm-exchange reactions, and they were thoroughly purified to remove extra free ligands. Before OAm exchange, the ZB-CdSe nanocrystals exhibited characteristic IR spectral features corresponding to oleic acid ligands being deprotonated and bonded onto their surface in the form of negatively charged oleate (Figure 2). The identification of deprotonated oleate ligands on ZB-CdSe nanocrystals is consistent with the recent results from NMR measurements by Hens and co-workers.[48] In addition, IR spectra can further provide structural information on the bonding between oleate ligands and surface Cd^{2+} ions. The asymmetric and symmetric stretching vibrations of the carboxylate group ($-COO^-$) appeared at 1531 and 1439 cm^{-1}, respectively (Figure 2). The gap between these two stretching vibrations is 92 cm^{-1}, which indicates that the carboxylate group bonded to a surface cadmium ion through a chelating bidentate interaction.[49,50]

After OAm exchange at room temperature, the IR spectrum of the resulting CdSe nanocrystals clearly shows the coexistence of oleate and OAm on these nanocrystals (Figure 2a). In addition, nanocrystal samples at different aging times exhibit IR spectra with vibrational peaks at nearly identical relative intensity ratios, indicating that room temperature aging does not affect the ratio between oleate and OAm ligands. The characteristic N−H bending vibration band appeared at 1559 cm^{-1} and the N−H stretching vibrations emerged as the weak and broad bands at the range of 3000−3300 cm^{-1} (Figure 2b). The asymmetric stretching band of the COO^- group blue-shifted to 1541 cm^{-1}, while its symmetric stretching band slightly red-shifted to 1435 cm^{-1} (Figure 2c). The gap between these two bands increased to 106 cm^{-1}, suggesting that the chelating bidentate interaction between the carboxylate group and surface Cd^{2+} ion were weakened in the presence of OAm. We attribute this effect to the formation of hydrogen bonding between oleate and OAm on the surface of CdSe nanocrystals.

Two possible bonding mechanisms have been proposed: (i) OAm bonds on the nanocrystals surface only through hydrogen bonding with oleate groups [Figure 2d(i)] and (ii) OAm bonds to the surface oleate through both hydrogen bonding and a coordinating bond to a surface Cd^{2+} ion [Figure 2d(ii)]. Although both mechanisms can result in the weakening of the bidentate interactions between oleate and surface Cd^{2+} ions, the second mechanism is more likely because it can lead to the modification of the surface electronic states of CdSe nanocrystals through partially donating the lone-pair electrons on the N atom of OAm to the empty orbital of the surface Cd^{2+} ion. This interaction can give rise to the formation of hole traps in the presence of oleate ligands, which is consistent with the significant PL quenching effect as observed above. In addition, the interaction seems also to affect the wave function overlapping between the $1S_e$ electron and $2S_{h3/2}$ hole, thus decreasing the extinction coefficient of the E_2 excitonic transition of the CdSe nanocrystals (Figure 1).

After the CdSe nanocrystals were annealed in the OAm exchange solution at 240 °C for 30 min, the two strong carboxylate stretching bands disappeared, whereas the N−H bending band remained (Figure 2c). The IR spectrum of the resulting nanocrystals is nearly identical to that of OAm-capped W-CdSe nanocrystals, demonstrating that OAm replaced oleate ligands from the nanocrystal surface after high-temperature annealing. This ligand-exchange process should be associated with the atomic rearrangement of the nanocrystal surface because the removal of negatively charged oleate ligands may be accompanied with the loss of excess surface Cd^{2+} ions. In addition, the shift of the N−H stretching bands of the CdSe nanocrystals suggests the change of bonding nature between the OAm ligands and the CdSe nanocrystal surface, which is consistent with surface atomic rearrangement (Figure 2b). Moreover, the observed ΔE_{12} decreasing and PL enhancing effects during high-temperature annealing should also relate to the loss of oleate ligands as well as nanocrystal surface atomic rearrangement; the nearly total loss of oleate ligands is associated with the minimal ΔE_{12} gap and the maximal PL quantum yield of the CdSe nanocrystals (Figure 1b).

Structural Characterization. TEM and XRD were used to determine whether or not the optical property changes of the ZB-CdSe nanocrystals are caused by ligand-exchange induced ZB-to-W crystal structural transformation. TEM observations show that no measurable change in shape, size, or size distribution can be identified between the ZB-CdSe nanocrystal samples before and after OAm exchange (Figure 3b,c). Both oleate- and OAm-capped ZB-CdSe nanocrystals have a spherical shape and a diameter of

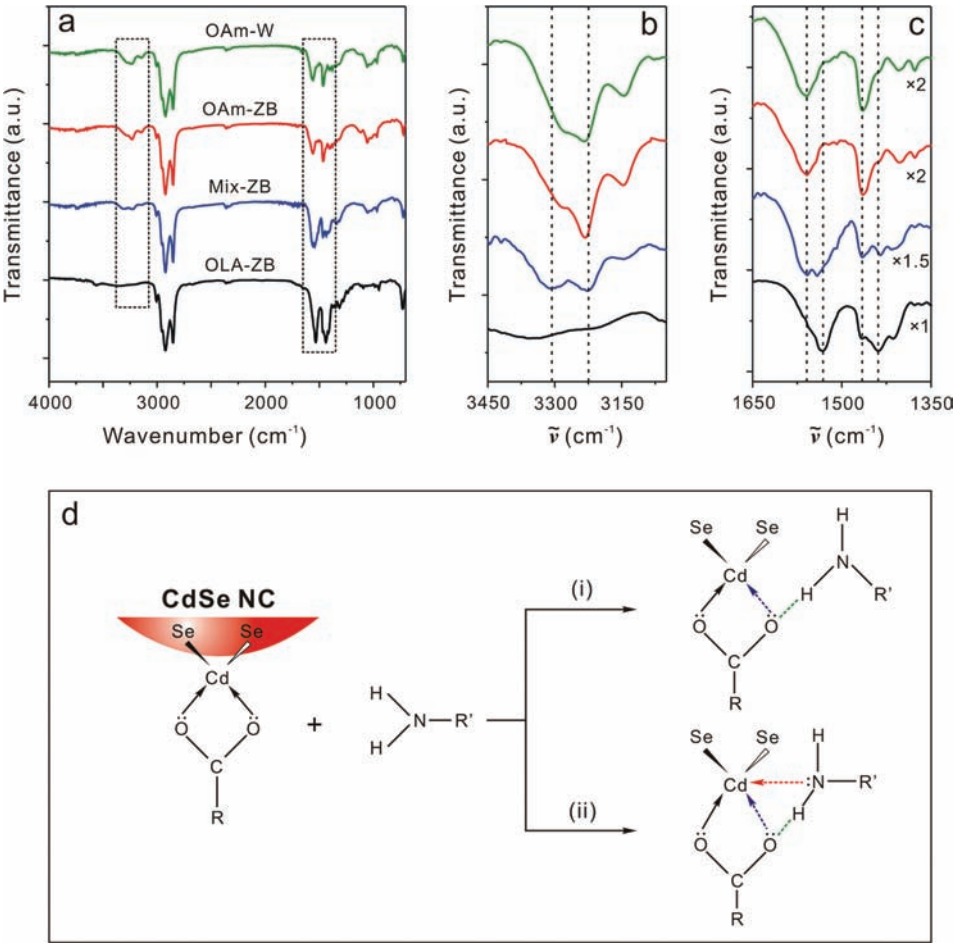

Figure 2. (a) FT-IR transmittance spectra of oleate-capped ZB-CdSe (black line), a mixture of OAm and oleate-capped ZB-CdSe (blue line), ZB-CdSe nanocrystals after ligand exchange reaction with OAm/ODE (red line), and OAm-capped W-CdSe nanocrystals (green line). (b) The zoomed-in FT-IR spectra of left highlighted area in part a. (c) The zoomed-in FT-IR spectra of right highlighted area in part a. (d) Proposed binding mechanisms of the ligand exchange reaction.

4.0 ± 0.2 nm; the size and size distribution of these nanocrystals are also nearly identical to those of the reference—the OAm-capped W-CdSe nanocrystals (Figure 3a). This result is consistent with that from the optical measurements, which show that the E_1 absorption and PL peaks of these three nanocrystal samples appear at nearly identical positions (Figure 1a).

Our XRD measurements show no evidence that OAm exchange can induce ZB-to-W crystal structural transformation. Like the oleate-capped ZB-CdSe nanocrystals, the OAm-capped CdSe nanocrystals exhibit characteristic features of a ZB crystal structure: (a) the valley between the (220) and (311) Bragg reflection peaks is deep, and (b) a discrete (400) Bragg peak appears at 61.0°.[41] A detailed comparison between these two XRD patterns shows that the OAm-capped ZB-CdSe nanocrystals have an additional (200) shoulder peak, indicating these nanocrystals exhibit a slightly better crystallinity than the oleate-capped nanocrystals (Figure 3d). In addition, the XRD patterns of these ZB-CdSe nanocrystals are clearly distinguishable from that of the OAm-capped W-CdSe nanocrystals, which exhibit the characteristic (102) and (103) Bragg peaks of a W-crystal structure.[19] Moreover, the (111) Bragg peak of the ZB-CdSe nanocrystals is evidently narrower than the first Bragg peak of the W-CdSe nanocrystals, which originates from a superposition of the (100), (002), and (101) Bragg peaks of a W-crystal structure (Figure 3d).[19]

However, a possibility still exists that the crystal structure of the ZB-CdSe nanocrystals just partially changed from a ZB to W phase, which cannot be easily distinguished by direct comparison of their XRD patterns. If this possibility did exist, the number of stacking faults inside these ZB-CdSe nanocrystals should increase accordingly because of the coexistence of the W stacking sequence (i.e., ABAB...). To test this possibility, we simulated the powder diffraction patterns following a literature method.[19,51] We built ZB-CdSe nanocrystals by stacking planes along the (111) axis of the ZB lattice and W-CdSe nanocrystals by stacking planes along the (0001) axis of the W lattice. A radius of 2 nm was used to carve out the nanocrystal assuming a spherical shape, and atomic coordinates were obtained by systematically generating atomic positions for a corresponding bulk crystal lattice and retaining only those atoms falling within the spherical nanocrystal. The XRD pattern of the nanocrystal was then calculated using a discrete form of the Debye equation[52]

$$I(S) = I_0 \frac{f^2(S)}{2\pi S} \sum_k \frac{p(r_k)}{r_k} \sin(2\pi r_k S) \quad (1)$$

where $I(S)$ is the diffracted intensity, I_0 is the incident intensity, $f(S)$ is the scattering factor, S is the scattering parameter, r_k is the

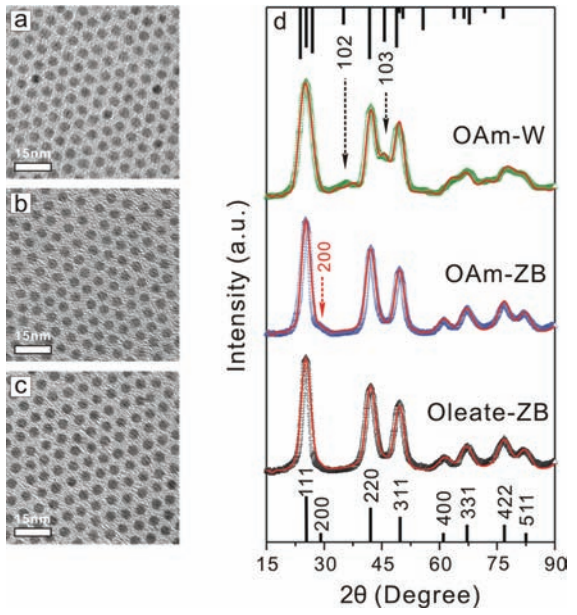

Figure 3. TEM images of (a) OAm-capped W-CdSe nanocrystals, (b) OAm-capped ZB-CdSe nanocrystals, (c) oleate-capped ZB-CdSe nanocrystals, (d) XRD patterns of OAm-capped W-CdSe nanocrystals (green open triangles), OAm-capped ZB-CdSe nanocrystals (blue open triangles), and oleate-capped ZB-CdSe nanocrystals (black open triangles). Red lines are the computer XRD simulation results. Stacking sequences applied for the simulations are the combination of ABCAB-CA*CBACBA (50%), ABCAB*AB*ACBACB (50%) for oleate-capped ZB-CdSe nanocrystals, ABCABCA*CBACBA (80%), ABCAB*AB*AC-BACB (20%) for OAm-capped ZB-CdSe nanocrystals, and ABA*CB-CBCBCBCB (20%), ABA*CBCBC*ACACA (80%) for OAm-capped W-CdSe nanocrystals (* indicating the position of the stacking fault in the given stacking sequence). The bottom and top stick patterns show the positions of standard XRD peaks for bulk ZB- and W-CdSe, respectively.

interatomic distance, and $p(r_k)$ is the number of times a given interatomic distance r_k occurs.

The simulated XRD patterns (Figure 3d, red lines) nearly perfectly reproduced the experimental data of all three types of CdSe nanocrystals in their Bragg peak positions, peak width, and even relative peak intensities (Figure 3d). The fit was obtained using the simulated XRD pattern for a weighted combination of two kinds of CdSe nanocrystal structures with the same radii, differing in the $(111)_{ZB}$ or $(0001)_W$ plane stacking sequence as detailed in the caption of Figure 3. The simulation shows that the 4.0-nm OAm-capped W-CdSe nanocrystals have an average of 1.8 stacking faults perpendicular to the $(0001)_W$ direction. There is an average of 1.5 stacking faults per particle along the $(111)_{ZB}$ direction in the 4.0-nm ZB CdSe nanocrystals before OAm exchange, whereas 1.2 stacking faults were found in the ZB-CdSe nanocrystals after OAm exchange. The slight decrease in stacking faults of OAm-capped ZB-CdSe nanocrystals is likely due to the high-temperature annealing during the ligand exchange reaction. Importantly, this simulation result rules out the possibility that partial ZB-to-W crystal transformation may occur in the core part of the ZB-CdSe nanocrystals during ligand exchange.

Isomaterial Core/Shell Growth of ZB-CdSe Nanocrystals. Although the average number of stacking faults inside the nanocrystals decreases after high-temperature OAm exchange, the surface layer of the CdSe nanocrystals may still undergo a partial change from ZB to W after OAm exchange. This small surface crystal structural change is normally undetectable using typical XRD measurements and simulations. To examine this possibility, we designed an isomaterial core/shell growth method in which a CdSe shell was grown on ZB-CdSe nanocrystals in a solution containing an OAm/ODE mixture (volume ratio 1:1). If a surface crystal structural change did occur during OAm exchange, the epitaxial CdSe shell should adopt a W-crystal structure. By increasing the thickness of the CdSe shell, the W-crystal structure should become the dominant structure of the resulting CdSe nanocrystals, which can be easily distinguished by XRD measurements.

In a typical isomaterial core/shell growth experiment, a hexane solution of oleate-capped ZB-CdSe nanocrystals (2.4 nm in diameter, 50 nmol) was added to an OAm/ODE (1:1, 5 mL) solution. After degassing and the removal of hexane, the resultant mixture was heated to 240 °C and 5.5 monolayers (ML) of CdSe shell were allowed to grow. Cadmium oleate and tributylphosphine selenide were used as the precursors. Before CdSe shell growth, OAm exchange occurred on the surface of the starting nanocrystals according to UV−vis absorption spectroscopy (Figure 4a). After 0.5 ML shell growth, the resulting CdSe nanocrystals displayed the absorption features and ΔE_{12} gap nearly identical to those of the OAm-capped W-CdSe nanocrystals with the same size (Figure 4a). With further CdSe shell growth, all excitonic absorption features of the resulting CdSe nanocrystals red-shifted. The overall shape of these multiple absorption features and their ΔE_{12} gaps kept nearly identical to those of high-quality OAm-capped W-CdSe nanocrystals of the same size, which were evidently distinguishable from those of oleate-capped ZB-CdSe nanocrystals of the same size (Figure 4a,b).

CdSe nanocrystals of 6.3 nm in diameter were obtained after 5.5-ML shell growth on the 2.4-nm ZB-CdSe nanocrystals; 94.5% of the materials in these 6.3-nm nanocrystals were built during the CdSe shell growth. If the OAm-exchange did induce a surface crystal structural change of ZB-CdSe nanocrystals, a major or at least distinguishable W structure is expected in the resulting CdSe nanocrystals, which should be easily identified by XRD. Experimental XRD data and simulation results show that the 2.4-nm CdSe nanocrystals (the starting core) possess a ZB-crystal structure with an average stacking fault of 0.8 along the (111) direction (Figure 4c), while the resulting 6.3-nm CdSe nanocrystals maintained a ZB-crystal form and had an average of 3.4 stacking faults (Figure 4d). This increased number of stacking fault should be associated with the significant volume increase of these CdSe nanocrystals, and this result is significant enough to rule out the possibility of ligand exchange induced surface crystal structural change.

Taken together, the results from optical measurements, XRD measurements, and simulation clearly demonstrate that OAm-exchange induced optical property changes are not caused by a ZB-to-W crystal structural change, but are associated with the chemical nature of the ligand as well as nanocrystal surface rearrangement due to the ligand exchange. In other words, the absorption feature differences between ZB- and W-CdSe nanocrystals are not due to the difference in their crystal structures, as we previously proposed.[41] To the best of our knowledge, these results provide the first unambiguous evidence that ligand exchange can cause a modification of the transition energy and extinction coefficient of an excitonic band of quantum-confined semiconductor nanocrystals.

It is worth noting that these results contradict Mahler's recent proposal that primary amine exchange can induce a crystal structure change in ZB-CdSe nanocrystals. Mahler et al. have

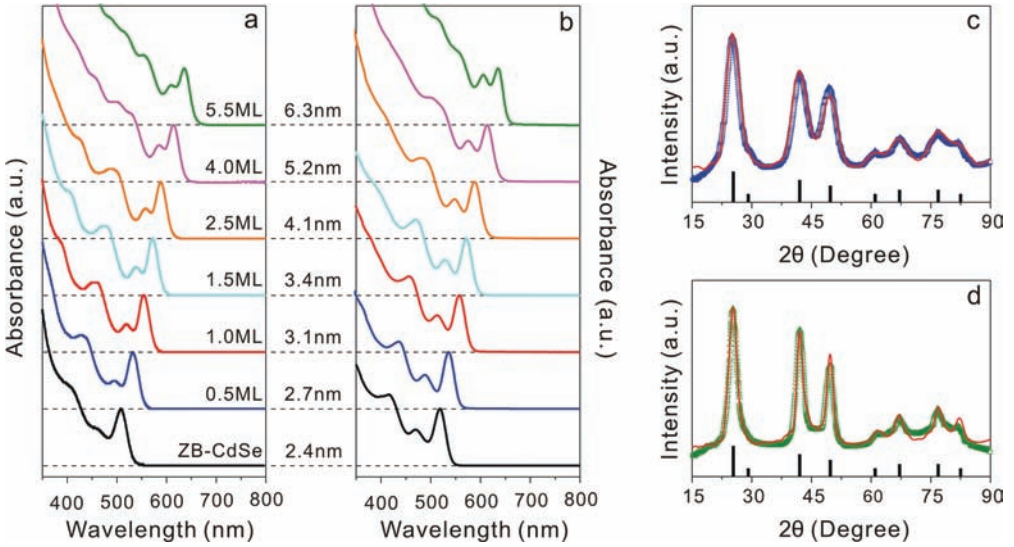

Figure 4. (a) Evolution of the absorption spectrum of the ZB-CdSe nanocrystals during the isomaterial core/shell growth. (b) The corresponding absorption spectra of oleate-capped ZB-CdSe nanocrystals. XRD patterns of starting ZB-CdSe nanocrystals (c, blue open triangles) and final CdSe/CdSe isomaterial core/shell nanocrystals (d, green open triangles). The simulation results are plotted by thin red lines in panels c and d. Stacking sequences applied for the simulations are the combination of ABCABCABC (20%), ABCAB*ACBA (80%) for 2.4 nm core CdSe nanocrystals and ABCAB*AB*ABCABC*BCABCA (60%) and ABCA*CBA*BCA*CBA*BCABCA (40%) for the 6.3-nm CdSe nanocrystals synthesized using isomaterial core/shell growth (* indicating the position of the stacking fault in the given stacking sequence).

recently discovered that, with the presence of a primary amine, the growth of thick CdS shell on small ZB-CdSe nanocrystals yielded final core/shell nanocrystals with a coexistence of both ZB and W crystal structures.[45] On the basis of our results from CdSe/CdSe isomaterial core/shell growth, we think that the coexistence of ZB and W structures in Mahler's CdSe/CdS core/shell nanocrystals should not be caused by a crystal structural change, but could just be due to the growth habit of CdS, which favors a W structure in the presence of primary fatty amines.[23]

Surface-Functionalization-Dependent Optical Properties of ZB-CdSe Nanocrystals of Different Sizes. To assess whether this ligand-exchange induced optical property change in CdSe nanocrystals is size-dependent, oleate-capped ZB-CdSe nanocrystals of four different sizes (i.e., 2.7, 3.3, 4.3, and 5.6 nm in diameter) were studied. Upon OAm exchange, all these ZB-CdSe nanocrystals exhibit similar optical changes to those in the 4.0-nm ZB-CdSe nanocrystals, as discussed above. After mixing these nanocrystals with an OAm/ODE (1:4) solution at room temperature, the extinction coefficient of their E_2 ($2S_{h3/2}1S_e$) band substantially decreased and the band appeared as a shoulder feature in their absorption spectra (Figure 5). After high-temperature OAm exchange, the peak positions of their E_1 excitonic band remained unchanged (the variations were within ±2 nm), whereas their ΔE_{12} gap narrowed to a value very close to that of OAm-capped W-CdSe nanocrystals (Figure 5). The ΔE_{12} gap narrowed from 247.7 to 187.7 meV for 2.7 nm nanocrystals, 200.1 to 149.6 meV for 3.3 nm nanocrystals, 151.6 to 116.4 meV for 4.3 nm nanocrystals, and 123.2 to 101.6 meV for 5.6 nm nanocrystals. These results show that the degree of this ΔE_{12} gap narrowing effect is size-dependent: the larger the size, the smaller the ΔE_{12} gap narrowed, and vice versa (Figure 5). In addition, our absorption spectroscopy study also shows that the OAm-capped ZB-CdSe nanocrystals made from isomaterial core/shell growth exhibit an identical size-dependent ΔE_{12} gap narrowing effect when compared with their oleate-capped counterparts (Figure 4a,b). Moreover, the OAm exchange also significantly

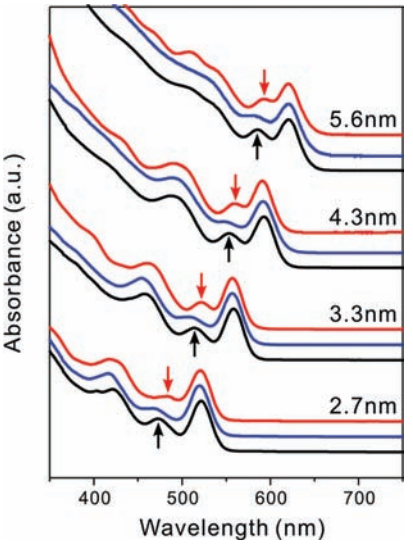

Figure 5. Absorption spectra of different size ZB-CdSe nanocrystals at three ligand exchange stages: oleate-capped ZB-CdSe nanocrystals (black line), OAm/oleate-capped ZB-CdSe nanocrystals (blue line), and OAm-Capped ZB-CdSe nanocrystals (red line).

modified the PL quantum yields of the CdSe nanocrystals, but not the peak position of their PL emission. The OAm exchange at room temperature led to a more than 95% decrease in their PL emissions, which is associated with the coexistence of oleate and OAm surface ligands. With the removal of oleate from the surface of these nanocrystals during annealing at 240 °C, their PL emissions were recovered and even enhanced as compared with those before OAm exchange. Interestingly, the PL emissions of the resulting OAm-capped CdSe nanocrystals were not sensitive to the OAm exchange at room temperature as their oleate-capped counterpart were. These results further demonstrate that

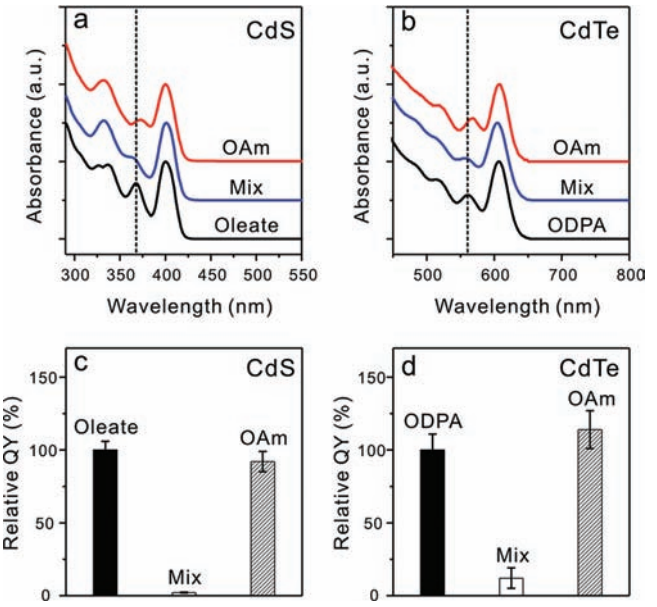

Figure 6. Absorption spectra of (a) CdS and (b) CdTe nanocrystals with different capping ligands: oleate or octadecyl-phosphonate (ODPA) (black line), OAm/oleate or OAm/ODPA (blue line), and OAm (red line). Relative PL QY of (c) CdS and (d) CdTe nanocrystals with different capping ligands: oleate or ODPA, OAm/oleate (Mix) or OAm/ODPA (Mix), and OAm.

OAm-capped CdSe nanocrystals have significantly different surface properties from oleate-capped nanocrystals, which can be attributed to the difference in the quantum confinement energies of the excitons in these two types of nanocrystals (vide infra).

Surface-Functionalization-Dependent Optical Properties of CdS and CdTe Nanocrystals. Our results further show that oleate-capped ZB-CdS nanocrystals and octadecyl-phosphonate-capped ZB-CdTe nanocrystals also exhibit surface-functionalization-dependent optical properties. Before OAm exchange, high-quality ZB-CdS nanocrystals (3.1 nm in diameter) exhibited a strong E_2 ($2S_{h3/2}1S_e$) excitonic absorption peak at 367 nm, and ZB-CdTe nanocrystals (4.0 nm in diameter) showed an E_2 absorption peak at 561 nm. After OAm exchange at room temperature, the position of the E_1 ($1S_{h3/2}1S_e$) absorption band of these two nanocrystals did not shift, but the extinction coefficients of their E_2 peaks decreased substantially (Figure 6a,b). No measurable shift was observed in the positions of their PL emission peaks, whereas the PL emission quantum yield decreased significantly: 98% decrease for the CdS nanocrystals and 88% decrease for the CdTe nanocrystals (Figure 6c,d). After further annealing at 240 °C, the E_1 bands of both nanocrystal showed virtually no shift, whereas the ΔE_{12} gap of the CdS nanocrystals narrowed from 279.4 to 229.4 meV and that of the CdTe nanocrystals narrowed from 167.9 to 144.5 meV. This process was also accompanied with the recovering of their PL emissions: the CdS nanocrystals showed 92% recovery in their PL emissions and the CdTe nanocrystals displayed slight PL enhancing to 114% when compared with those before OAm exchange (Figure 6c,d).

Theoretical Modeling of the Electronic Structure. The objective herein is to gain further insights into the OAm-exchange-induced red shift of the E_2 absorption band (or ΔE_{12} gap narrowing) of these oleate (or octadecyl-phosphonate) capped II−VI semiconductor nanocrystals. A common characteristic of these nanocrystals is that their surface is functionalized with

Scheme 1. Scheme of Ligand Effects on the Electronic Structure of a CdSe Nanocrystal[a]

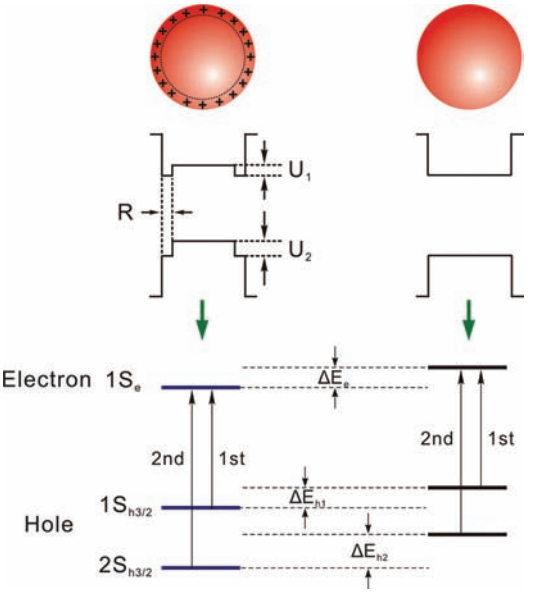

[a] R is the type II shell thickness of the positively charged thin layer generated by oleate. U_1 (U_2) is the potential barrier for the electron (hole) generated by this thin type II shell. ΔE_e is the shift of the lowest electron energy state ($1S_e$) from that of the CdSe nanocrystal with an OAm-capped neutral surface. ΔE_{h1} and ΔE_{h2} are the shifts of hole energy states ($1S_{h3/2}$, $2S_{h3/2}$) compared to that of the particle with OAm-capped neutral surface.

anionic ligands, and thus a thin layer of excess cations (i.e., Cd^{2+}) should exist on their surface to balance to charges of the negatively charged ligands, making them overall neutral nanocrystals.[48,53] We hypothesize that the existence of an excess Cd^{2+} ion surface layer creates a very thin type II CdSe shell with its valence and conduction bands slightly lower than the inside CdSe core, and this thin type II shell is removed after the anionic ligands are replaced with the neutral OAm. On the basis of this hypothesis, we used a spherical box model to calculate the confinement energies of electrons and holes in CdSe nanocrystals before and after OAm exchange (Scheme 1).[54]

In this model the electron and hole wave functions were treated separately.[54] There were three radial potential regions in the oleate-capped type II core/shell nanocrystals (i.e., core, shell, and the surrounding organic layer), whereas two radial potential regions were used in the OAm-capped nanocrystals (i.e., core and the surrounding organic layer, Scheme 1). We calculated the quantum-confinement energies of the lowest electronic state ($1S_e$) and the $1S_{h3/2}$ and $2S_{h3/2}$ hole states by solving the continuity relationship of the electron and hole wave functions and probability currents at the interfaces (eqs 2 and 3).[54,55]

$$R_{1S,\,core}(k_1 r_1) = R_{1S,\,shell}(k_2 r_1) \tag{2}$$

$$\frac{1}{m^*_{core}}\frac{d}{dr}R_{1S,\,core}(k_1 r)\bigg|_{r=r_1} = \frac{1}{m^*_{shell}}\frac{d}{dr}R_{1S,\,shell}(k_2 r)\bigg|_{r=r_1} \tag{3}$$

where $R_{1S,core}$ and $R_{1S,shell}$ are the lowest energy radial wave functions for electron or hole in the CdSe core and type II CdSe

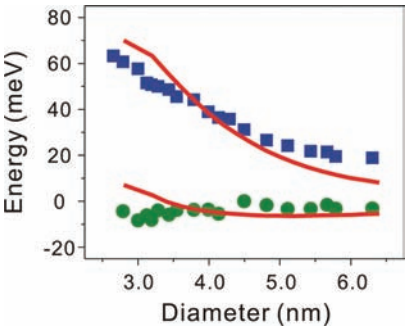

Figure 7. The energy differences of the first absorption band (ΔE_1, green dots) and the second absorption band (ΔE_2, blue squares) between the oleate-capped and OAm-capped CdSe nanocrystals as a function of crystal diameter. The red lines are the calculated energy shift of the first and second absorption bands using the parameters of R = 0.4 nm, $U_1 = -0.08$ eV, and $U_2 = 0.27$ eV.

shell, respectively, r_1 is the radius of the CdSe core, m^*_{core} and m^*_{shell} are the bulk effective masses of electron or hole in the CdSe core and type II CdSe shell, respectively, and k_1 and k_2 are the wave vectors in the CdSe core and type II CdSe shell.

In the calculations, we used the effective masses and dielectric constants of the bulk CdSe,[56] a barrier height of 4.0 eV for the surrounding organic layer for the electron, and 1.0 eV for the hole. Our results show that the existence of a thin type II shell decreases the $1S_e$ energy by ΔE_e and increases the $1S_{h3/2}$ and $2S_{h3/2}$ energies by ΔE_{h1} and ΔE_{h2} but broadens the energy difference between these two hole states. OAm exchange-induced absorption-feature changes in these nanocrystals are associated with the removal of the type II shell, and therefore, their E_1 absorption peak shift (ΔE_1) is equal to $\Delta E_{h1} - \Delta E_e$, and their E_2 peak shift (ΔE_2) is $\Delta E_{h2} - \Delta E_e$.

To gain a quantitative understanding of OAm exchange-induced surface effects, we further calculated ΔE_1 and ΔE_2 as a function of nanocrystal size. Importantly, the calculation of energy difference can substantially cancel out the systematic errors originated from the simplicity of the spherical box model used herein. When using a shell thickness of 0.4 nm, $U_1 = -0.08$ eV, and $U_2 = 0.27$ eV, the size-dependent ΔE_1 and ΔE_2 values obtained by this simple theoretical modeling appear to be in a good agreement with our experimental data (Figure 7). These results indicate that the size dependence of ΔE_{12} gap narrowing in these CdSe nanocrystals is due to the quantum confinement effect and the existence of a thin type II shell.

The existence of a thin type II shell on oleate-capped CdSe nanocrystals could also cause other optical property changes that were observed during OAm exchange. With this thin type II shell, the kinetic energy of the $2S_{h3/2}$ hole increases substantially, and thus the wave function of this hole can strongly couple with that of the lone electron pairs on the nitrogen atom of OAm. This strong coupling effect can result in the decrease of the oscillation strength (or extinction coefficient) of the E_2 excitonic transition and the quenching of the PL emission of CdSe nanocrystals when the coexistence of oleate and OAm surface ligands occurred in the stage of the OAm exchange at room temperature. During the high-temperature treatments, the thin type II shell on these nanocrystals can be gradually removed with the replacement of oleate ligands by OAm, which can lead to the monotonic red shift of the E_2 peak and the recovering and enhancing of their PL emissions (Figure 1 and Figure 6c,d).

CONCLUSIONS

We report the unambiguous identification that II−VI semiconductor nanocrystals exhibit surface-functionalization-dependent excitonic absorption features. Our results show that the transition energy and extinction coefficient of the E_2 ($2S_{h3/2}1S_e$) excitonic band of these nanocrystals can be strongly modified by their surface ligands as well as ligand-associated surface atomic arrangement. The OAm exchange of oleate-capped ZB II−VI nanocrystals leads to a narrowing of their ΔE_{12} gap, and this ΔE_{12} gap narrowing effect is size-dependent. This OAm exchange process is also accompanied by the quenching and recovering of the PL emission of these nanocrystals. In addition, the results from our XRD measurements and simulations completely rule out the possibility that OAm exchange can give rise to a ZB-to-W crystal structure transformation in the core or on the surface of ZB-CdSe nanocrystals. Moreover, our theoretical modeling suggests that the surface-functionalization-dependent optical properties of these semiconductor nanocrystals may originate from a thin isomaterial type II shell which is created by the anionic oleate or octadecyl-phosphonate ligands.

ASSOCIATED CONTENT

Supporting Information. Detailed synthetic procedures. This material is available free of charge via the Internet at http://pubs.acs.org.

AUTHOR INFORMATION

Corresponding Author
cao@chem.ufl.edu

ACKNOWLEDGMENT

We thank Major Analytical Instrumentation Center (MAIC) at the University of Florida for TEM and XRD usage. Y.C.C. acknowledges the NSF (DMR-0645520 Career Award) and the ONR (N00014-09-1-0441).

REFERENCES

(1) Bawendi, M. G.; Carroll, P. J.; Wilson, W. L.; Brus, L. *J. Chem. Phys.* **1992**, *96*, 946.
(2) Alivisatos, A. P. *J. Phys. Chem.* **1996**, *100*, 13226.
(3) Kuno, M.; Lee, J. K.; Dabbousi, B. O.; Mikulec, F. V.; Bawendi, M. G. *J. Chem. Phys.* **1997**, *106*, 9869.
(4) Kovalenko, M. V.; Scheele, M.; Talapin, D. V. *Science* **2009**, *324*, 1417.
(5) Shimizu, K. T.; Woo, W. K.; Fisher, B. R.; Eisler, H. J.; Bawendi, M. G. *Phys. Rev. Lett.* **2002**, *89*, 117401.
(6) Mahler, B.; Spinicelli, P.; Buil, S.; Quelin, X.; Hermier, J. P.; Dubertret, B. *Nat. Mater.* **2008**, *7*, 659.
(7) Wang, X.; Ren, X.; Kahen, K.; Hahn, M. A.; Rajeswaran, M.; Zacher, S. M.; Silcox, J.; Cragg, G. E.; Efros, A. L.; Krauss, T. D. *Nature* **2009**, *459*, 686.
(8) Wang, C.; Shim, M.; Guyot-Sionnest, P. *Science* **2001**, *291*, 2390.
(9) Munro, A. M.; Plante, I, J.; Ng, M. S.; Ginger, D. S. *J. Phys. Chem. C* **2007**, *111*, 6220.
(10) Frederick, M. T.; Weiss, E. A. *ACS Nano* **2010**, *4*, 3195.
(11) Hines, M. A.; Guyot-Sionnest, P. *J. Phys. Chem.* **1996**, *100*, 468.
(12) Reiss, P.; Protière, M.; Li, L. *Small* **2009**, *5*, 154.
(13) Peng, X.; Schlamp, M. C.; Kadavanich, A. V.; Alivisatos, A. P. *J. Am. Chem. Soc.* **1997**, *119*, 7019.

(14) Li, J. J.; Wang, Y. A.; Guo, W.; Keay, J. C.; Mishima, T. D.; Johnson, M. B.; Peng, X. *J. Am. Chem. Soc.* **2003**, *125*, 12567.
(15) Reiss, P.; Bleuse, J.; Pron, A. *Nano Lett.* **2002**, *2*, 781.
(16) Alivisatos, P. *Science* **1996**, *271*, 933.
(17) Yin, Y.; Alivisatos, A. P. *Nature* **2005**, *437*, 664.
(18) Bruchez, M.; Moronne, M.; Gin, P.; Weiss, S.; Alivisatos, A. P. *Science* **1998**, *281*, 2013.
(19) Murray, C. B.; Norris, D. J.; Bawendi, M. G. *J. Am. Chem. Soc.* **1993**, *115*, 8706.
(20) Medintz, I. L.; Uyeda, H. T.; Goldman, E. R.; Mattoussi, H. *Nat. Mater.* **2005**, *4*, 435.
(21) Cao, Y. C.; Wang, J. *J. Am. Chem. Soc.* **2004**, *126*, 14336.
(22) Du, H.; Chen, C.; Krishnan, R.; Krauss, T. D.; Harbold, J. M.; Wise, F. W.; Thomas, M. G.; Silcox, J. *Nano Lett.* **2002**, *2*, 1321.
(23) Peng, Z. A.; Peng, X. *J. Am. Chem. Soc.* **2001**, *123*, 183.
(24) Pradhan, N.; Reigsnyder, D.; Xie, R. G.; Aldana, J.; Peng, X. *J. Am. Chem. Soc.* **2007**, *129*, 9500.
(25) Talapin, D. V.; Haubold, S.; Rogach, A. L.; Kornowski, A.; Haase, M.; Weller, H. *J. Phys. Chem. B* **2001**, *105*, 2260.
(26) Yu, J. H.; Joo, J.; Park, H. M.; Baik, S. I.; Kim, Y. W.; Kim, S. C.; Hyeon, T. *J. Am. Chem. Soc.* **2005**, *127*, 5662.
(27) Yu, W.; Falkner, J. C.; Shih, B. S.; Colvin, V. L. *Chem. Mater.* **2004**, *16*, 3318.
(28) Hines, M. A.; Scholes, G. D. *Adv. Mater.* **2003**, *15*, 1844.
(29) Murphy, J. E.; Beard, M. C.; Norman, A. G.; Ahrenkiel, S. P.; Johnson, J. C.; Yu, P. R.; Mićić, O. I.; Ellingson, R. J.; Nozik, A. J. *J. Am. Chem. Soc.* **2006**, *128*, 3241.
(30) Xu, S.; Kumar, S.; Nann, T. *J. Am. Chem. Soc.* **2006**, *128*, 1054.
(31) Medintz, I. L.; Uyeda, H. T.; Goldman, E. R.; Mattoussi, H. *Nat. Mater.* **2005**, *4*, 435.
(32) Han, M.; Gao, X.; Su, J. Z.; Nie, S. *Nat. Biotechnol.* **2001**, *19*, 631.
(33) Mews, A.; Zhao, J. *Nat. Photon* **2007**, *1*, 683.
(34) Coe, S.; Woo, W. K.; Bawendi, M. G.; Bulović, V. *Nature* **2002**, *420*, 800.
(35) Kazes, M.; Lewis, D. Y.; Ebenstein, Y.; Mokari, T.; Banin, U. *Adv. Mater.* **2002**, *14*, 317.
(36) Zhu, L.; Zhu, M.; Hurst, J. K.; Li, A. D. Q. *J. Am. Chem. Soc.* **2005**, *127*, 8968.
(37) Talapin, D. V.; Murray, C. B. *Science* **2005**, *310*, 86.
(38) Chen, Y.; Vela, J.; Htoon, H.; Casson, J. L.; Werder, D. J.; Bussian, D. A.; Klimov, V. I.; Hollingsworth, J. A. *J. Am. Chem. Soc.* **2008**, *130*, 5026.
(39) Pandey, A.; Guyot-Sionnest, P. *Science* **2008**, *322*, 5903.
(40) Norris, D. J.; Bawendi, M. G. *Phys. Rev. B* **1996**, *53*, 16338.
(41) Yang, Y. A.; Wu, H.; Williams, K. R.; Cao, Y. C. *Angew. Chem., Int. Ed.* **2005**, *44*, 6712.
(42) Mohamed, M. B.; Tonti, D.; Al-Salman, A.; Chemseddine, A.; Chergui, M. *J. Phys. Chem. B* **2005**, *109*, 10533.
(43) Capek, R. K.; Moreels, I.; Lambert, K.; Muynck, D. D.; Zhao, Q.; Tomme, A. V.; Vanhaecke, F.; Hens, Z. *J. Phys. Chem. C* **2010**, *114*, 6371.
(44) Chen, O.; Chen, X.; Yang, Y.; Lynch, J.; Wu, H.; Zhuang, J.; Cao, Y. C. *Angew. Chem., Int. Ed.* **2008**, *47*, 8638.
(45) Mahler, B.; Lequeux, N.; Dubertret, B. *J. Am. Chem. Soc.* **2010**, *132*, 953.
(46) Peng, X.; Wickham, J.; Alivisatos, A. P. *J. Am. Chem. Soc.* **1998**, *120*, 5343.
(47) Li, R.; Lee, J.; Yang, B.; Horspool, D. N.; Aindow, M.; Papadimitrakopoulos, F. *J. Am. Chem. Soc.* **2005**, *127*, 2524.
(48) Fritzinger, B.; Capek, R. K.; Lambert, K.; Martins, J. C.; Hens, Z. *J. Am. Chem. Soc.* **2010**, *132*, 10195.
(49) Wu., N; Fu, L.; Su, M.; Aslam, M.; Wong, K. C.; Dravid, V. P. *Nano Lett.* **2004**, *4*, 383.
(50) Wu, H.; Yang, Y.; Cao, Y. C. *J. Am. Chem. Soc.* **2006**, *128*, 16522.
(51) Cao, Y.; Banin, U. *Angew. Chem., Int. Ed.* **1999**, *38*, 3692.
(52) Hall, B. D.; Monot, R. *Comput. Phys.* **1991**, *5*, 414.
(53) Owen, J. S.; Park, J.; Trudeau, P. E.; Alivisatos, A. P. *J. Am. Chem. Soc.* **2008**, *130*, 12279.
(54) Dabbousi, B. O.; Rodriguez-Viejo, J.; Mikulec, F. V.; Heine, J. R.; Mattoussi, H.; Ober, R.; Jensen, K. F.; Bawendi, M. G. *J. Phys. Chem. B* **1997**, *101*, 9463.
(55) Atkins, P.; De Paula, J. *Physical Chemistry*, 9th ed.; Oxford Univeristy Press: New York, 2010.
(56) Madelung, O. *Semiconductors: Data Handbook*, 3rd ed.; Springer: New York, 2003.